ICCM2012
November 25-28, 2012, Gold Coast, Australia
www.ICCM-2012.org

Solution methods for advection-diffusion-reaction equations on growing domains and subdomains, with application to modelling skin substitutes

M. P. Adams*[1,2], D. G. Mallet[1,2], G. J. Pettet[1,2]
[1]*Mathematical Sciences School, Queensland University of Technology, Brisbane, Queensland, Australia*
[2]*Institute of Health and Biomedical Innovation,*
Queensland University of Technology, Brisbane, Queensland, Australia
**Corresponding author: mp.adams@qut.edu.au*

Abstract

Problems involving the solution of advection-diffusion-reaction equations on domains and subdomains whose growth affects and is affected by these equations, commonly arise in developmental biology. Here, a mathematical framework for these situations, together with methods for obtaining spatio-temporal solutions and steady states of models built from this framework, is presented. The framework and methods are applied to a recently published model of epidermal skin substitutes. Despite the use of Eulerian schemes, excellent agreement is obtained between the numerical spatio-temporal, numerical steady state, and analytical solutions of the model.

Keywords: Growing domain; Nonuniform growth; Continuum; Epithelium; Skin substitute

1. Introduction

During biological development, the growth characteristics of tissue domains such as bone, muscle, skin or other epithelia can fundamentally affect their final form. Mathematical models have shown that the form of tissue domain growth critically modifies the appearance of skin colour patterns of the marine angelfish *Pomacanthus* (Painter, 2001), skeletal pattern formation in chick limb (Dillon and Othmer, 1999), tangential growth of the *Drosophila* wing disc (Baker and Maini, 2007) and the ability of migratory cells to fully colonise a tissue domain (Simpson *et al.*, 2006). Most of these models prescribe a simple form to the domain growth (linear, exponential, logistic, etc.). However, species kinetics on the domain may also contribute to the growth pattern of these tissues (Niswander *et al.*, 1994; Baker and Maini, 2007).

In addition, the growth characteristics of adjacent tissues are often intrinsically linked during their development. For example, the *in vitro* growth and deterioration of epidermal skin substitutes (Gibbs *et al.*, 1997) is likely to depend on the exchange of cells and chemical signals between this tissue's four distinct sublayers (Adams *et al.*, 2012). Biological tissue may also split into distinct subdomains during development, as in the teeth primordia of *Alligator mississippiensis* (Kulesa *et al.*, 1996). For these situations, a mathematical framework for the growth and development of connected subdomains is required.

Hence in this paper, we present a mathematical framework and solution methods for the modelling of species evolution on one-dimensional growing domains and subdomains. In this framework, which builds upon the work of Crampin *et al.* (1999), the domain and subdomain growth may depend on species kinetics, and vice versa. Strategies are presented for obtaining numerical solutions of these spatio-temporal models, as well as the less numerically-intensive identification of their steady states. Finally, an application of the mathematical framework to a recent model of the growth of epidermal skin substitutes (Adams *et al.*, 2012) is demonstrated.

2. Problem Statement

Consider a system of m advection-diffusion-reaction equations, describing changes in species $C_i(z,t)$, $i = 1,\ldots,m$, that act on a one-dimensional growing domain $0 \le z \le L(t)$,

$$\frac{\partial C_i}{\partial t} + \frac{\partial}{\partial z}\left(v_i C_i - D_i \frac{\partial C_i}{\partial z} \right) = R_i, \qquad i = 1,...,m, \tag{1}$$

where each equation is subject to an initial condition $C_i(z,0)$ and an appropriate number of boundary conditions at $z = 0$ and $z = L(t)$ so that unique and consistent solutions are obtained. In Eq. (1), v_i, D_i, and R_i represent the advective velocity, diffusion coefficient and reaction term respectively for each species $C_i(z,t)$. Typically the expression for v_i contains a term representing the local tissue velocity, a result easily shown by application of Reynolds' transport theorem (Crampin *et al.*, 1999; Painter, 2001). There are also n subdomains within $0 \le z \le L(t)$,

$$0 \le z \le z_1(t); \qquad z_{j-1}(t) < z \le z_j(t), \qquad j = 2,...,n, \tag{2}$$

defined by the stationary boundary at $z = 0$ and mobile boundaries $z_j(t)$, $j = 1,\ldots,n$, where $z_n(t) = L(t)$. The change in position of each mobile boundary $z_j(t)$ is described by some function f_j,

$$\frac{dz_j}{dt} = f_j, \qquad j = 1,...,n, \tag{3}$$

together with its initial condition $z_j(0)$. The functions v_i, D_i, R_i and f_j may depend linearly or nonlinearly on z, t, any of the species $C_i(z,t)$, or any of the boundary locations $z_j(t)$.

3. Obtaining a Spatio-Temporal Solution

To obtain a solution of Eq. (1), we uniformly transform the growing domain $0 \le z \le L(t)$ to a stationary domain $0 \le z^* \le 1$, according to $(z,t) \to (z^*,t^*) = (z/L(t),t)$ where (z^*,t^*) are the coordinates in the stationary domain (Crampin *et al.*, 1999). We rewrite Eq. (1)-(3) in terms of this stationary domain (z^*,t^*), and drop asterisks for notational simplicity,

$$\frac{\partial C_i}{\partial t} + \frac{\partial}{\partial z}\left(\frac{v_i - f_n z}{L} C_i - \frac{D_i}{L^2}\frac{\partial C_i}{\partial z} \right) = R_i - \frac{f_n}{L} C_i, \qquad i = 1,...,m, \tag{4}$$

$$0 \le z \le \alpha_1(t); \qquad \alpha_{j-1}(t) < z \le \alpha_j(t), \qquad j = 2,...,n-1; \qquad \alpha_{n-1}(t) < z \le 1, \tag{5}$$

$$\frac{d(\alpha_j L)}{dt} = f_j, \qquad j = 1,...,n. \tag{6}$$

Here the subdomain boundaries are represented by $\alpha_j(t^*) = z_j(t)/L(t)$, $j = 1,\ldots,n$, and the replacement $dL/dt = f_n$ in Eq. (4) follows from Eq. (3) and the relation $z_n(t) = L(t)$.

Eq. (4)-(6) are written on a stationary domain, and thus can be solved using standard numerical methods for ordinary (Burden and Faires, 2010) and partial differential equations (Morton and Mayers, 2005). In particular, for certain advection-dominated problems the Kurganov-Tadmor operator split algorithm, proposed by Simpson *et al.* (2006), is recommended for solution of Eq. (4). However, we found for our application (modelling epidermal skin substitutes) that Eulerian methods were sufficient.

4. Obtaining a Steady State Solution

Stationary steady states $t \to \infty$ of the system in Eq. (1)-(3) can be identified as follows. Steady states are obtained by setting all temporal derivatives to zero and solving the equations

$$\frac{\partial}{\partial z}\left(v_i C_i - D_i \frac{\partial C_i}{\partial z} \right) - R_i = 0, \qquad i = 1,...,m, \tag{7}$$

$$f_j = 0, \qquad j = 1,...,n. \tag{8}$$

Solutions of Eq. (7) and (8) yield final states of the species distributions $C_i(z, t \to \infty)$ and the final positions of mobile boundaries $z_j(t \to \infty)$ respectively. Functions f_j in Eq. (8), which are equal to the velocity of boundaries z_j in Eq. (3), may for the purposes of solution here be replaced by *any* function equal to zero that uniquely determines the location of the associated mobile boundary z_j and depends only on z, t, any C_i, and/or any z_j.

Because the location of mobile boundaries z_j and distribution of species C_i may depend on each other we solve Eq. (7) and (8) together using the following procedure:

1. Make initial estimates for the steady state positions of all mobile boundaries z_j, $j = 1,\ldots,n$.
2. Using these z_j, numerically solve the ordinary differential equations in Eq. (7) and hence obtain the set of functions f_j that we wish to make equal to zero (see Eq. (8)).
3. Employ an appropriate root-finding algorithm to use the obtained functions f_j to update the estimates of mobile boundary locations z_j.
4. Repeat Steps 2 and 3 until Eq. (8) is satisfied within appropriate tolerances.

If there are multiple stationary steady states of Eq. (1)-(3), different initial estimates of the boundary locations z_j chosen in Step 1 may be required to identify them. It is also conceivable that a solution of Eq. (7) and (8) is not a physically reasonable final state of the system because it is an unstable node. If all eigenvalues associated with the linearisation of Eq. (7) and (8) about the steady state in question are negative, the steady state corresponds to a possible final stationary state of Eq. (1)-(3) (Edelstein-Keshet, 1998).

5. Application: Modelling Epidermal Skin Substitutes

5.1 The model

We recently investigated the growth and deterioration of human epidermal skin substitutes with a mathematical model built from the framework defined in Section 2 (Adams *et al.*, 2012). With this model we investigated a possible explanation for why epidermal substitutes *in vitro* reduce significantly in thickness and become unusable within only a few weeks (Gibbs *et al.*, 1997), whilst *in vivo* epidermis maintains fairly constant thickness during its lifetime. Because calcium is strongly implicated in regulating the multilayered structure of the epidermis (Hennings *et al.*, 1980), and because it has been recently shown that tight junctions regulate the epidermal calcium distribution

(Kurasawa *et al.*, 2011), the model examined whether or not abnormalities in tight junction regulation of epidermal calcium could explain the discrepancy between the epidermal growth patterns *in vivo* and *in vitro*.

The skin substitute model consists of four species (corresponding to C_i, i = 1,2,3,4): intracellular calcium ρ_{ci}, extracellular calcium ρ_{ce}, tight junctions T and a hypothetical signal chemical S. Each species is described by an advection-diffusion-reaction equation, an initial condition, and an appropriate number of boundary conditions. The spatial domain encloses the living component of the epidermal skin substitute, and the number of subdomains m (which corresponds to the number of living epidermal sublayers) changes at distinct times t_{12} and t_{23} triggered by specific local events. These distinct times define three model stages: in Stage 1 ($0 \le t \le t_{12}$) there are three subdomains, in Stage 2 ($t_{12} < t \le t_{23}$) there are four subdomains, and in Stage 3 ($t > t_{23}$) there are also four subdomains but a boundary condition for the species S changes.

In particular, the equations governing the model are:

$$\frac{\partial \rho_{ci}}{\partial t} = \begin{cases} 0, & 0 \le z \le \theta z_1, \\ g_c(\rho_{ce}, z_2) - \dfrac{\partial}{\partial z}(\rho_{ci} u_i), & \theta z_1 < z \le z_3, \end{cases} \qquad \rho_{ci}(z,0) = \rho_{ci}(0,t) = \rho_{i0}, \tag{9}$$

$$\frac{\partial \rho_{ce}}{\partial t} = \frac{\partial}{\partial z}\left(D_C(T) \frac{\partial \rho_{ce}}{\partial z} \right) - g_c(\rho_{ce}, z_2), \qquad \rho_{ce}(z,0) = \rho_{e0},$$

$$\rho_{ce}(0,t) = \rho_{e0}, \qquad D_C(T(L,t)) \frac{\partial \rho_{ce}}{\partial z}(L,t) = \rho_{ce}(L,t) \frac{dL(t)}{dt}, \tag{10}$$

$$\frac{\partial S}{\partial t} = \frac{\partial}{\partial z}\left(D_S(T) \frac{\partial S}{\partial z} - S u_i \right), \qquad S(z,0) = 0, \qquad S(0,t) = 0, \qquad S(L,t) = \begin{cases} 0, & t < t_{23}, \\ 1, & t \ge t_{23}, \end{cases} \tag{11}$$

$$\frac{\partial T}{\partial t} = g_T(S, T, z_2) - \frac{\partial}{\partial z}(T u_i), \qquad T(z,0) = 0, \qquad T(0,t) = 0. \tag{12}$$

Stage 1 starts at time $t = 0$. The domain is divided by boundaries $z = 0$, θz_1, z_1, z_2 into three subdomains, with positions governed by:

$$\frac{d(\theta z_1)}{dt} = \frac{dz_1}{dt} = 0, \qquad \frac{dz_2}{dt} = u_i(z_2), \qquad z_2(0) = z_1. \tag{13}$$

Stage 2 starts at time $t = t_{12}$ when $\rho_{ci}(z_2) \ge \rho_{\text{diff}}$. The domain is divided by boundaries $z = 0$, θz_1, z_1, z_2, z_3 into four subdomains, with positions governed by:

$$\frac{d(\theta z_1)}{dt} = \frac{dz_1}{dt} = 0, \qquad z_2 \in \operatorname{argmin}_{z_2} \left\{ \rho_{ci}(z_2) \ge \rho_{\text{diff}}, \ \frac{dz_2}{dt} = u_i(z_2) \right\},$$

$$\frac{dz_3}{dt} = u_i(z_3), \qquad z_3(t_{12}) = z_2(t_{12}). \tag{14}$$

Stage 3 starts at time $t = t_{23}$ when $\rho_{ci}(z_3) = 0$. The domain is divided by boundaries $z = 0$, θz_1, z_1, z_2, z_3 into four subdomains, with positions governed by:

$$\frac{d(\theta z_1)}{dt} = \frac{dz_1}{dt} = 0, \qquad z_2 \in \text{argmin}_{z_2}\left\{\rho_{ci}(z_2) \geq \rho_{\text{diff}},\ \frac{dz_2}{dt} = u_i(z_2)\right\},$$

$$z_3 \in \text{argmin}_{z_3}\left\{\rho_{ci}(z_3) = 0,\ \frac{dz_3}{dt} = u_i(z_3)\right\}. \qquad (15)$$

In the skin substitute model expressed by Eq. (9)-(15), the precise form of diffusion coefficients $D_C(T)$, $D_S(T)$, advection due to the local cell velocity $u_i(z)$, reaction terms $g_c(\rho_{ce}, z_2)$, $g_T(S, T, z_2)$, and constants ρ_{i0}, ρ_{e0}, and ρ_{diff}, are given in Adams *et al.* (2012). For the subsequent discussion we do not require any further information about these functions and constants, except to note that $u_i(z)$ is always positive for $z > 0$, and $D_C(T) = D_{Ca}(1 - (1 - \varepsilon_{Ca})T)$ where D_{Ca} and ε_{Ca} are constants.

In Eq. (14) and (15), the argmin expressions indicate that the minimum value of z_j from its two values calculated from the two equations inside the curly brackets, is chosen. In their current form, Eq. (14) and (15) do not adhere to the form prescribed in Eq. (3), but their numerical implementations do:

$$\frac{\Delta z_2}{\Delta t} = \min\left\{\frac{z\big|_{\rho_{ci}=\rho_{\text{diff}}} - z_2}{\Delta t}, u_i(z_2)\right\}, \quad \frac{\Delta z_3}{\Delta t} = \min\left\{\frac{z\big|_{\rho_{ci}=0} - z_3}{\Delta t}, u_i(z_3)\right\}, \qquad (16)$$

where $z\big|_{\rho_{ci}=\rho_{\text{diff}}}$ and $z\big|_{\rho_{ci}=0}$ indicate spatial positions z where $\rho_{ci}(z) = \rho_{\text{diff}}$ and $\rho_{ci}(z) = 0$ respectively.

Eq. (9)-(15) represent a system in which the growth kinetics of connected subdomains are not easily separated from the species kinetics acting on these subdomains, a situation which is likely to be common in developmental biology (Niswander *et al.*, 1994). In Stages 2 and 3 of the model, the mobile boundaries z_2 and z_3 depend partially on the species distribution ρ_{ci} as shown by Eq. (14) and (15). In turn, changes in the positions of z_2 and z_3 modify reaction terms for ρ_{ci}, ρ_{ce} and T, and the boundary conditions for ρ_{ce} and S respectively, as shown by Eq. (9)-(12).

The physical consequences of this model have been discussed in a previous paper (Adams *et al.*, 2012). Here, we demonstrate how the methods described in Sections 3 and 4 were applied to obtain numerical spatio-temporal and steady state solutions of the model. The validity of these methods is verified by an inter-code comparison between these numerical solutions and an analytical solution which is applicable if D_{Ca} is sufficiently high ($\geq 10^{-9}$ m^2 s^{-1}, data not shown).

5.2 Spatio-temporal solution

For the spatio-temporal solution of Eq. (9)-(15) obtained by following the methods described in Section 3, the stationary boundaries θz_1 and z_1 become mobile in the transformed coordinate system (z^*, t^*) due to the dependence of their transformed positions on the domain boundary $L(t)$ (given by $z_2(t)$ in Stage 1 and $z_3(t)$ in Stages 2 and 3). The advection-diffusion-reaction equations (9)-(12) were discretised using the Crank-Nicholson method with second-order central differences for diffusion terms and first-order upwinding for advection terms (Morton and Mayers, 2005). The mobile boundary equations (13)-(15) were solved using the explicit Euler method and updated synchronously on the same timestep as the species kinetics.

Because the advection-diffusion-reaction equations are nonlinear, the Newton-Armijo method (Kelley, 2003) was employed in tandem with the Crank-Nicholson method for their solution. The Newton-Armijo method requires the calculation of matrix inverses, and if Eq. (9)-(12) are solved simultaneously with this method these matrices become exceeding large and computational time dramatically increases. By taking into account the interdependence of species ρ_{ci}, ρ_{ce}, S and T in Eq. (9)-(12), we used the following implementation of these methods to reduce the size of matrices to be inverted and hence minimise computational time:

1. At each timestep, Eq. (11) and (12) for S and T were solved simultaneously using the Crank-Nicholson and Newton-Armijo methods because they contain no dependence on ρ_{ci} or ρ_{ce}. This step can be skipped in Stages 1 and 2 of the model because in these stages $S = T = 0$.
2. Within the same timestep, Eq. (10) for ρ_{ce} was solved using the Crank-Nicholson and Newton-Armijo methods because ρ_{ce} depends only on T and itself.
3. Finally, Eq. (9) for ρ_{ci} was solved using only the Crank-Nicholson method because its dependence on itself is linear.

5.3 Steady state solution

To obtain steady state solutions of Eq. (9)-(15), assumed to occur only in Stage 3 of the model, we followed the four-step procedure set out in Section 4. Because this procedure does not require any coordinate transformation, only two mobile boundaries z_2 and z_3 need to be determined simultaneously with the species distributions. Hence, in Step 1 only the locations of z_2 and z_3 need to be estimated. For Step 2, time-dependence was removed from Eq. (9)-(12) and the resulting system of ordinary differential equations, which possess boundary conditions at both $z = 0$ and $z = z_3$, was transformed to an iteratively-converging sequence of initial value problems using the nonlinear shooting method (Burden and Faires, 2010). These initial value problems were solved numerically using the explicit Euler method.

In the argmin expressions of Eq. (15), steady positions of z_2 and z_3 cannot correspond to the second equations $dz_j / dt = u_i(z_j)$, $j = 2,3$, because $u_i(z) > 0$ for $z > 0$. Hence the functions f_j that we wish to make equal to zero follow from the first equations within these argmin expressions, and can be written as

$$f_1(z_2, z_3) = \rho_{ci}(z_2) - \rho_{\text{diff}} = 0, \qquad f_2(z_2, z_3) = \rho_{ci}(z_3) = 0. \tag{17}$$

For Step 3, the root-finding algorithm we used to solve Eq. (17) was again the Newton-Armijo method (Kelley, 2003), which for this situation requires the calculation of f_1, f_2, $\partial f_1/\partial z_2$, $\partial f_1/\partial z_3$, $\partial f_2/\partial z_2$ and $\partial f_2/\partial z_3$ evaluated at the current estimate of z_2 and z_3. Hence, in each iteration of Step 3 we calculated five values each for f_1 and f_2 evaluated at (z_2, z_3), $(z_2 + \Delta z/2, z_3)$, $(z_2 - \Delta z/2, z_3)$, $(z_2, z_3 + \Delta z/2)$ and $(z_2, z_3 - \Delta z/2)$ to determine $f_1(z_2, z_3)$ and $f_2(z_2, z_3)$ and approximate the required partial derivative terms according to:

$$\left.\frac{\partial f_j}{\partial z_2}\right|_{(z_2,z_3)} \approx \frac{1}{\Delta z}\left(f_j\left(z_2 + \frac{\Delta z}{2}, z_3\right) - f_j\left(z_2 - \frac{\Delta z}{2}, z_3\right)\right), \quad j = 1,2, \tag{18}$$

$$\left.\frac{\partial f_j}{\partial z_3}\right|_{(z_2,z_3)} \approx \frac{1}{\Delta z}\left(f_j\left(z_2, z_3 + \frac{\Delta z}{2}\right) - f_j\left(z_2, z_3 - \frac{\Delta z}{2}\right)\right), \quad j = 1,2. \tag{19}$$

This requires five separate solutions of Eq. (9)-(12) with time-dependence removed, in Step 2. Finally, the tolerances required in Step 4 simply consist of the relative and absolute tolerances associated with the Newton-Armijo method (Kelley, 2003).

5.4 Results

We compared numerical spatio-temporal, numerical steady state and analytical (where applicable) solutions of the model expressed by Eq. (9)-(15) for the four parameter sets spanned by the choices of $D_{Ca} = 10^{-11}$ m^2 s^{-1}, 10^{-9} m^2 s^{-1} and $\varepsilon_{Ca} = 5 \times 10^{-5}$, 1 with all other parameters at the fixed values reported in Adams *et al.* (2012). Of these four sets, the best match between solution methods was obtained for $(D_{Ca}, \varepsilon_{Ca}) = (10^{-9}$ m^2 s^{-1}, 1) and the worst match was obtained for $(D_{Ca}, \varepsilon_{Ca}) = (10^{-11}$ m^2 s^{-1}, $5 \times 10^{-5})$. Hence, the solutions of Eq. (9)-(15) for these two parameter sets are presented in Fig. 1. For $(D_{Ca}, \varepsilon_{Ca}) = (10^{-9}$ m^2 s^{-1}, 1), numerical spatio-temporal (red), numerical steady state (pink), and analytical (black) solutions are shown. For $(D_{Ca}, \varepsilon_{Ca}) = (10^{-11}$ m^2 s^{-1}, $5 \times 10^{-5})$, only numerical spatio-temporal (blue) and numerical steady state (cyan) solutions are plotted, as the applicability condition of sufficiently high D_{Ca} required for an analytical solution is not satisfied for this parameter set.

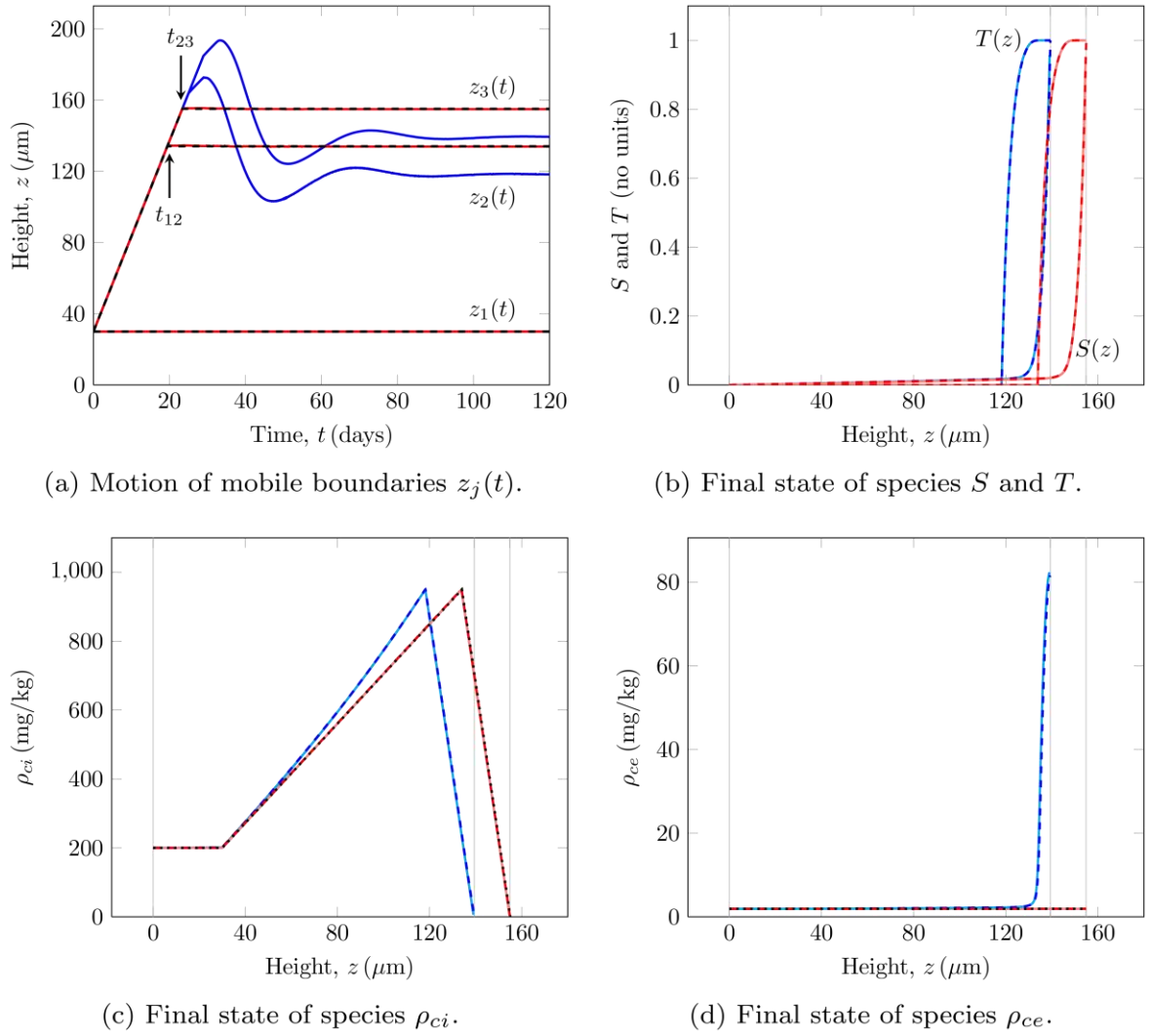

(a) Motion of mobile boundaries $z_j(t)$.

(b) Final state of species S and T.

(c) Final state of species ρ_{ci}.

(d) Final state of species ρ_{ce}.

Figure 1. Analytical (black) and numerical (red, pink, blue, cyan) solutions of the skin substitute model.

Fig. 1 demonstrates that the numerical spatio-temporal and steady state solutions, generated using the methods described in Sections 3 and 4, match extremely well with each other and with the analytical solution (where applicable). Fig. 1(a) shows that the temporal change in boundaries $z_2(t)$ and $z_3(t)$ match well between the analytical and numerical spatio-temporal solutions for $(D_{Ca}, \varepsilon_{Ca}) = (10^{-9}\ \mathrm{m}^2\ \mathrm{s}^{-1}, 1)$. In addition, the predicted final boundary locations $z_2(t \to \infty)$ and $z_3(t \to \infty)$ varied between solution methods by less than 0.4%, for all four parameter sets (data not shown). Figs. 1(b)-(d) show that all final species distributions matched well between solution methods. These results demonstrate the suitability of the presented numerical spatio-temporal and steady state solution methods to this skin substitute model.

We also investigated the convergence of the steady state solution method, by calculating steady state distributions of all species and boundaries for $D_{Ca} = 10^{-11}\ \mathrm{m}^2\ \mathrm{s}^{-1}, 10^{-9}\ \mathrm{m}^2\ \mathrm{s}^{-1}$ and 1001 values of ε_{Ca} spaced equally on a logarithmic scale from 10^{-5} to 1 (2002 simulations total, data not shown). We found that the convergence of the Newton-Armijo method to identify these steady states depended strongly on the initial estimates chosen for z_2 and z_3. Hence, for the steady state method we implemented the following addition to the solution algorithm: if the Armijo rule is invoked more than 10 times during a Newton step, new initial guesses for z_2 and z_3 are chosen at random such that $100\ \mu\mathrm{m} \leq z_2 < z_3 \leq 180\ \mu\mathrm{m}$ and the steady state solution process restarts from the beginning. For all 2002 simulations, initial estimates z_2 and z_3 could always be found so that the steady state solution method converged within high tolerances to the correct values of the final boundary locations.

6. Discussion

For the skin substitute model we found that graphs of the numerical spatio-temporal, numerical steady state and (if applicable) analytical solutions were visibly indistinguishable. This strong agreement is particularly surprising for the species distributions T and ρ_{ci}, whose absence of diffusion and hence infinite Péclet numbers are expected to yield severe dissipation in Eulerian schemes (Simpson *et al.*, 2006). This dissipation depends strongly on the spatial discretisation (Morton and Mayers, 2005), and yet our numerical spatio-temporal and steady state solutions were indistinguishable despite the use of vastly different spatial discretisations ($L/\Delta z = 10^3$ and $L/\Delta z = 10^5$ respectively). Although we and other groups (Baker *et al.*, 2009) have observed success with Eulerian schemes in growing domain problems, we caution that the validity of numerical results for these problems should always be carefully examined, either by comprehensive inter-code comparisons, the use of robust methods such as the Kurganov-Tadmor operator split algorithm proposed by Simpson *et al.* (2006), or testing against analytical solutions where possible.

During the identification of steady states for our skin substitute model, we found that the convergence of the Newton-Armijo method depended strongly on the initial estimates chosen for z_2 and z_3. This most likely occurs because f_1 and f_2, whose zeros are sought in this method, depend in a complex fashion via the solution of four ordinary differential equations on z_2 and z_3, but we have not investigated this further. Hence the examination of alternative root-finding algorithms to the Newton-Armijo method, for the identification of steady states arising from advection-diffusion-reaction kinetics on growing domains, is a possible extension to this work.

There are some limitations to the mathematical framework presented here. We assumed that the functions v_i, D_i, R_i and/or f_j in Eq. (1)-(3) cannot depend on spatial or temporal derivatives of $C_i(z, t)$ or $z_j(t)$. However, the functions v_i typically depend on the local tissue velocity (Crampin *et al.*, 1999; Painter, 2001), which due to the subdomain growth may in turn depend on temporal derivatives of mobile boundaries z_j. Additionally, in models of chemotactic and diffusive cell migration on

growing domains, cell advection may depend on the local chemoattractant gradient (Simpson *et al.*, 2006). In these situations, spatio-temporal solutions may still be obtained using the transformation described in Section 3, but Eq. (4) is no longer correct. However, the steady state procedure described in Section 4 is unaffected and hence is still suitable for these problems.

On the other hand, the skin substitute model demonstrates that the proposed model framework allows the emergence of new spatial subdomains at later times, by dividing the temporal domain into model stages as in Eq. (13)-(15). This has immediate application, for example, to models of the lower jaw of *Alligator mississippiensis* in which successive partitioning of the spatial domain contributes crucially to the formation of the first seven teeth primordia (Kulesa *et al.*, 1996). Regardless of the application, it is hoped that the present work will contribute to the formation of future mathematical models in developmental biology.

References

Adams, M. P., Mallet, D. G. and Pettet, G. J. (2012), A continuum model of the growth of engineered epidermal skin substitutes. *ANZIAM J. (EMAC 2011)* 53, pp. C90–C109.

Baker, R. E. and Maini, P. K. (2007), A mechanism for morphogen-controlled domain growth. *Journal of Mathematical Biology* 54, pp. 597–622.

Baker, R. E., Yates, C. A. and Erban, R. (2009), From microscopic to macroscopic descriptions of cell migration on growing domains. *Bulletin of Mathematical Biology* 72, pp. 719–762.

Burden, R. L. and Faires, J. D. (2010), *Numerical analysis*, 9th edition, Brooks/Cole.

Crampin, E. J., Gaffney, E. A. and Maini, P. K. (1999), Reaction and diffusion on growing domains: scenarios for robust pattern formation. *Bulletin of Mathematical Biology* 61, pp. 1093–1120.

Dillon, R. and Othmer, H. G. (1999), A mathematical model for outgrowth and spatial patterning of the vertebrate limb bud. *Journal of Theoretical Biology* 197, pp. 295–330.

Edelstein-Keshet, L. (1988), *Mathematical models in biology*, Mc-Graw Hill.

Gibbs, S., Vičanová, J., Bouwstra, J., Valstar, D., Kempenaar, J. and Ponec, M. (1997), Culture of reconstructed epidermis in a defined medium at 33°C shows a delayed epidermal maturation, prolonged lifespan and improved stratum corneum. *Archives of Dermatological Research* 289, pp. 585–595.

Hennings, H., Michael, D., Cheng, C., Steinert, P., Holbrook, K. and Yuspa, S. H. (1980), Calcium regulation of growth and differentiation of mouse epidermal cells in culture. *Cell* 19, pp. 245–254.

Kelley, C. T. (2003), *Solving nonlinear equations with Newton's method*, Society for Industrial and Applied Mathematics.

Kulesa, P. M., Cruywagen, G. C., Lubkin, S. R., Maini, P. K., Sneyd, J., Ferguson, M. W. J. and Murray, J. D. (1996), On a model mechanism for the spatial patterning of teeth primordia in the alligator. *Journal of Theoretical Biology* 180, pp. 287–296.

Kurasawa, M., Maeda, T., Oba, A., Yamamoto, T. and Sasaki, H. (2011), Tight junction regulates epidermal calcium ion gradient and differentiation. *Biochemical and Biophysical Research Communications* 406, pp. 506–511.

Morton, K. W. and Mayers, D. F. (2005), *Numerical solution of partial differential equations*, 2nd edition, Cambridge University Press.

Niswander, L., Jeffrey, S., Martin, G. R. and Tickle, C. (1994), A positive feedback loop coordinates growth and patterning in the vertebrate limb. *Nature* 371, pp. 609–612.

Painter, K. J. (2001), Models for pigment pattern formation in the skin of fishes, chapter in: Maini, P. K. and Othmer, J. G. (editors), *Mathematical models for biologic pattern formation*, Springer-Verlag, pp. 59–82.

Simpson, M. J., Landman, K. A. and Newgreen, D. F. (2006), Chemotactic and diffusive migration on a nonuniformly growing domain: numerical algorithm development and applications. *Journal of Computational and Applied Mathematics* 192, pp. 282–300.